Triple-Band Microstripline-Fed Printed Wide-Slot Antenna for WiMAX/WLAN Operations

Mustafa H. B. Ucar [1] and Yunus E. Erdemli [2]

[1] Information Systems Engineering Department, Faculty of Technology
Kocaeli University, Umuttepe, 41380 Kocaeli, Turkey
mhbucar@kocaeli.edu.tr

[2] Biomedical Engineering Department, Faculty of Technology
Kocaeli University, Umuttepe, 41380 Kocaeli, Turkey
yunusee@koceli.edu.tr

Abstract ─ A novel triple-band microstrip antenna design is introduced for WiMAX/WLAN applications. The proposed antenna has a moderate size of $38 \times 39 \times 0.79$ mm^3, yet offers quite well gain performance (5.6-8 dBi) over the operational bands. The antenna consists of a microstrip feed-line coupled to a pair of concentric rectangular loops, as well as a split-ring element inserted within a slotted ground plane, which may also be considered as a wide-slot antenna element. In the paper, the numerical antenna design along with the corresponding measurement results is presented. An equivalent circuit modeling of the proposed design along with empirical formulae relating antenna parameters with notch frequencies is also introduced to serve as a useful design guideline.

Index Terms ─ Empirical formulae, equivalent circuit modeling, loop element, microstripline feed, multiband operation, printed wide-slot antenna, split-ring element, WiMAX, WLAN.

I. INTRODUCTION

Today's rapidly evolving modern wireless communication systems are experiencing unprecedented changes. This wave of changes leads to drive increasing importance and demand of multiband compact antennas in the wireless systems; namely, Worldwide Inter-operability for Microwave Access (WiMAX) and Wireless Local Area Network (WLAN). These services offer multiband fast-access with a high mobility at either local/wide scale, and require compact printed antenna elements. In general, conventional printed monopoles, dipoles, or slots are shown to exhibit inherent narrow bandwidth characteristics. Hence, it is necessary to tailor either feed structure or antenna element, or both to achieve desired wideband and/or multiband operation. Particularly, multiband operation is preferred to avoid possible interferences from the other communication systems which share the same frequency bands.

Recent studies have led to a variety of promising multi-band [1]-[11] printed antennas to meet WLAN/WiMAX requirements in general. In particular, the designs in [5]-[9] offer triple-band WiMAX/WLAN operations, which is also the scope of this paper. Considering those triple-band designs, an expected tradeoff between antenna size and gain performance is observed as can be seen from Table 1. Particularly, the antenna design of ref. [8] allows for an almost 3 dB gain enhancement as compared to that of ref. [5], while the latter design is almost half in size of the former design.

Table 1: Antenna size and gain comparison

Ref. No	Size (mm^3)	Gain (dBi)
[5]	$20 \times 27 \times 1$	1.8-2.78
[6]	$36 \times 30 \times 1.6$	3.27-5.0
[7]	$40 \times 40 \times 0.8$	1.77-4.13
[8]	$50 \times 50 \times 1$	4-6

In this study, we introduce a novel triple-band microstrip antenna design for WiMAX/WLAN applications. The multiband antenna has a

moderate size of 38×39×0.79 mm^3, or equivalently, the electrical size is ~0.3 λ_0×0.3 λ_0 and ~0.75 λ_0×0.75 λ_0 at the operational frequencies of 2.4 GHz and 5.95 GHz, respectively. More importantly, the proposed antenna provides much better gain performance (5.6-8 dBi) over the operational bands, while being comparable in size to its counterparts reported in [5]-[9]. In the paper, the numerical antenna design along with the corresponding measurement results is presented. We note that the full-wave analysis of the proposed design has been carried out using CST Microwave Studio.

In this study, we also introduce a simplistic equivalent circuit model for the proposed antenna, along with empirical formulae relating some design parameters and the notch frequencies to assist engineering design. In particular, equivalent circuit modeling offers a systematic way of design approach, and the related studies are available in the literature for simple antenna structures [12], [13]. However, it may be difficult to consider such analyses for rather complex configurations; e.g., our case. We therefore, offer a preliminary equivalent circuit model based on integration of previously reported simple models [14], [15]. In addition, we have derived empirical formulae relating some design parameters and the notch frequencies for the proposed triple-band antenna, which is expected to serve as an additional design perspective. A similar synthesis was previously reported for an ultra-wideband antenna [16].

The proposed triple-band antenna design is moderate-size, low-loss, low-cost, and provides flatter and better gain profile over the bands of interest compared to the aforementioned counterparts. Besides the antenna's satisfactory performance, we believe that the introduced empirical formulae along with the proposed equivalent circuit model are additional contributions of this research.

II. ANTENNA DESIGN

The triple-band antenna configuration is shown in Fig. 1, along with its physical parameters. As seen in Fig. 1, the slotted ground plane (*W*×*L*) is etched on a low-loss (tanδ=0.0009) thin substrate with a thickness of *h*=0.79 mm and

ε_r=2.2. The proposed antenna is comprised of a stepped microstrip feed-line coupled to a pair of concentric rectangular loops as well as a split-ring element inserted within a slotted ground plane, which may also be considered as a wide-slot antenna element as depicted in Fig. 1. The rectangular wide-slot element (*W*$_s$×*L*$_s$) is excited by a stepped microstripline placed on other side of the substrate. The feedline is designed to have two sections with 50 Ω (*W*$_f$×*L*$_f$) and ~100 Ω (*W*$_h$×*L*$_h$) characteristic impedances, so as to serve for broadband matching to 50 Ω system. Also, two strip loadings (*W*$_c$×*L*$_c$) are located on each side of the feedline for the purpose of better impedance matching, particularly in the third operational band.

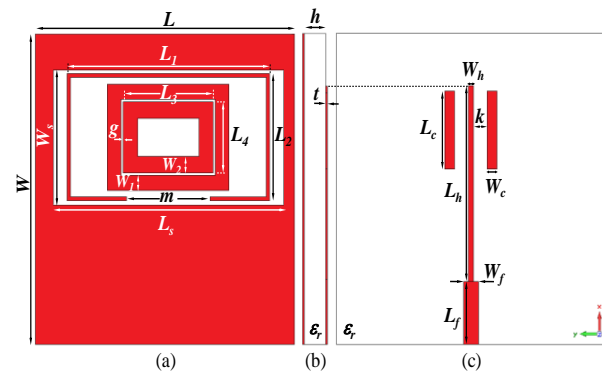Fig. 1. The proposed antenna configuration: (a) front, (b) side, (c) back views; *h*=0.79, *W*=39, *L*=38, *L*$_s$=33, *W*$_s$=18.5, *t*=0.05, *L*$_1$=29, *L*$_2$=16, *L*$_3$=13, *L*$_4$=9, *W*$_1$=2, *W*$_2$=2.1, *W*$_f$=2.2, *W*$_h$=0.8, *W*$_c$=1.4, *L*$_c$=9.7, *L*$_h$=24.4, *L*$_f$=8, *g*=0.2, *m*=12, *k*=1.9 (all in mm), ε_r=2.2.

Multiband antenna operation can be achieved due to inherent antenna structure as reported in [5], [6], and [8]. However, to suppress dispensable bands, additional parasitic elements or loadings (e.g.: strips, slots, rings, etc.) may be utilized within a wide-band antenna design to realize multiband WiMAX/WLAN operation [7]. Here, we employ a similar design approach to form notch bands by inserting parasitic elements into the wide-band antenna design. Hence, three design steps depicted in Fig. 2 have been employed to reach the final triple-band antenna configuration.
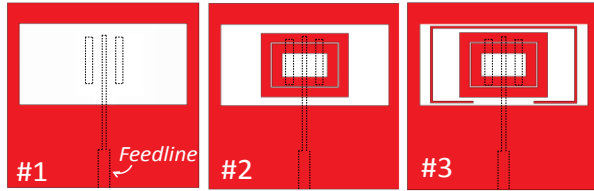
Fig. 2. The design steps for the proposed antenna configuration.

The simulated VSWR characteristics for the configurations #1, #2 and #3 are displayed in Fig. 3. At the beginning, the design #1 is obtained by means of a wide-slot antenna element coupled to a microstripline feed structure, resulting in a wideband VSWR<2 performance over 2.1-6.8 GHz band, as can be seen from Fig. 3. At the second stage, two concentric rectangular loops within the slot element are included to achieve the design #2, while introducing two notch-bands around 4.5 GHz and 6.3 GHz, owing to the outer and inner loops, respectively [4]; thus, resulting in a dual-band operation centered around 3.0 GHz and 5.5 GHz. Finally, a thin split-ring element is also placed around the double-loop element for the purpose of an additional notch-band centered at 3.1 GHz; hence, allowing for a triple-band operation with center frequencies of 2.6/3.5/5.5 GHz, while suppressing unused bands to avoid possible interferences. Consequently, the ultimate design #3 results in a triple-band operation; i.e., 2-2.96 GHz, 3.2-3.8 GHz and 5.05-6.12 GHz, which covers all the designated WLAN (2.4-2.48/5.15-5.35/5.72-5.82 GHz) and WiMAX (2.5-2.69/3.4-3.69/5.25-5.85 GHz) bands.
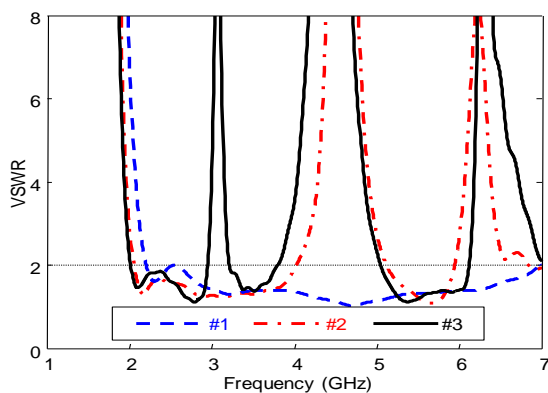

Fig. 3. The simulated VSWR characteristics of the corresponding design steps #1, #2 and #3, as depicted in Fig. 2.

III. RESULTS & DISCUSSIONS

The proposed triple-band antenna was fabricated on an Arlon DiClad 880 thin substrate (h=0.79 mm, ε_r=2.2), as shown in Fig. 4. The corresponding simulated and measured VSWR characteristics are displayed in Fig. 5.

As can be seen from Fig. 5, there is a fairly good agreement between the simulated and measured VSWR results with some expected discrepancies, due to possible material and fabrication tolerances. Of importance, is that the fabricated antenna provides the triple-band WiMAX/WLAN operation (2-2.9/3.2-3.63/5-6.2 GHz) where the notch-bands around 3.1 GHz, 4.5 GHz and 6.3 GHz are observed. We note that the VSWR measurements were carried out using Rohde & Schwarz ZVB8 Vector Network Analyzer.
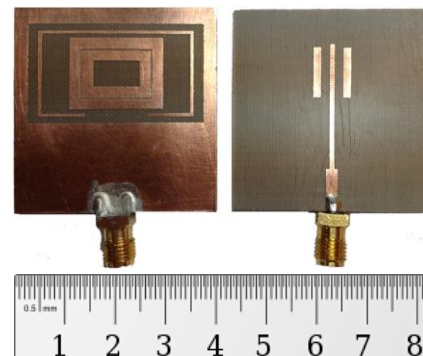

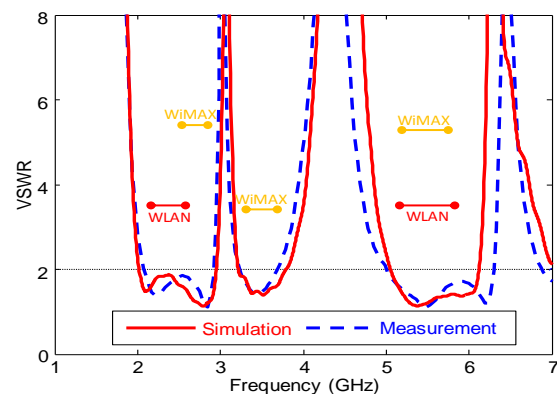Fig. 4. The front and back views of the fabricated antenna.

Fig. 5. The simulated and measured VSWR characteristics of the proposed antenna.

Figure 6 shows the computed surface current distributions at the centre frequencies of the notch-

bands; i.e., 3.1/4.5/6.3 GHz. As can be seen, the current distribution at 3.1 GHz is mainly concentrated over the split-ring element, while the distributions at 4.5 GHz and 6.3 GHz are predominantly highlighted around the outer and inner loops. In fact, those results confirm that the lower (3.1 GHz), the middle (4.5 GHz) and the upper (6.3 GHz) notch-bands occur by means of the presence of the split-ring, the outer loop, and the inner loop elements, respectively. As a result, by introducing those parasitic elements, possible undesired interferences at the specified notch-bands can be eliminated; thus, distortion-free communication can be achieved.
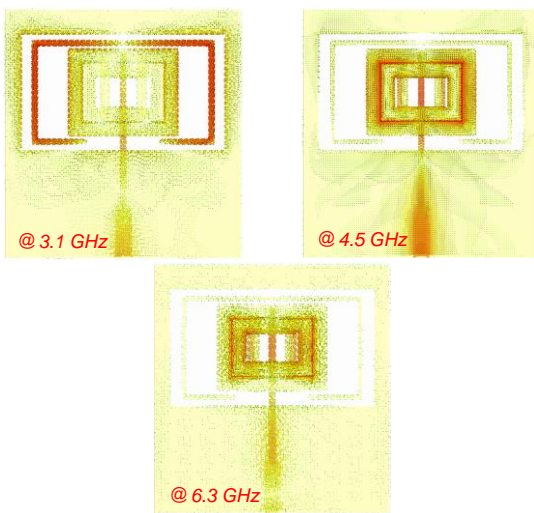

Fig. 6. The simulated surface current distributions at the centre frequencies of the notch-bands.

We also carried out radiation pattern measurements using A-INFO LB-880 DRG horn antenna (0.8-8 GHz) in a non-isolated laboratory environment. The measured patterns along with the simulations at the operational frequencies of 2.6 GHz, 3.5 GHz and 5.5 GHz are displayed in Fig. 7, where a reasonable agreement is observed. As can be seen, the antenna has almost omni-directional patterns in the H-plane and bidirectional patterns in the E-plane. Also, note that the simulated cross-polarization levels are negligible in the E-plane, while the H-plane cross-polarization levels increase with respect to increasing operating frequencies [17].
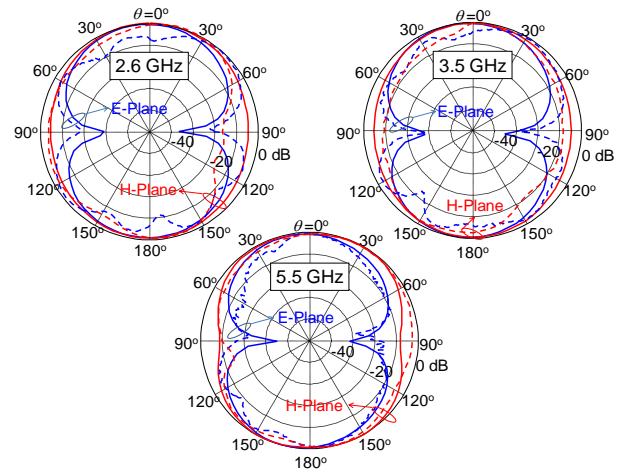

Fig. 7. The computed (solid) and measured (dashed) radiation patterns of the triple-band antenna at the center frequencies of 2.6/3.5/5.5 GHz.

Figure 8 shows the simulated realized-gain (IEEE gain × mismatch losses) characteristics for the antenna designs #1, #2 and #3 (see Fig. 2). As shown, the triple-band design (#3) has gain levels of 5.6-6.4 dBi, 6.6-6.8 dBi, and 6-8 dBi over the operational bands of 2-2.96 GHz, 3.2-3.8 GHz, and 5.05-6.12 GHz, respectively; whereas, expected gain dips occur at the designated notch-bands, owing to the parasitic elements (i.e.: split-ring and double-loop). Moreover, the measured gain has been calculated using the Friis Transmission Equation [18] for several frequency points, as shown in Fig. 8. We remark that the measured gains agree fairly well with the simulated ones over the operational bands, while some differences are observed in the notch bands with noting that a scant measurement setup was employed.

Furthermore, we extracted the measured efficiency (e_{cd}) using the measured gain (G), the measured mismatch losses ($e_m = 1 - |S_{11}|^2$) and the corresponding directivities (D_o) along with the formulation $G = e_{cd} \times e_m \times D_o$. For instance, the measured efficiency values at the frequencies of 2.6 GHz, 3.5 GHz, and 5.5 GHz are calculated as 97%, 95%, and 94%, which agree quite well with the simulated radiation efficiencies of 98%, 95%, and 97%. We note that possible dielectric and

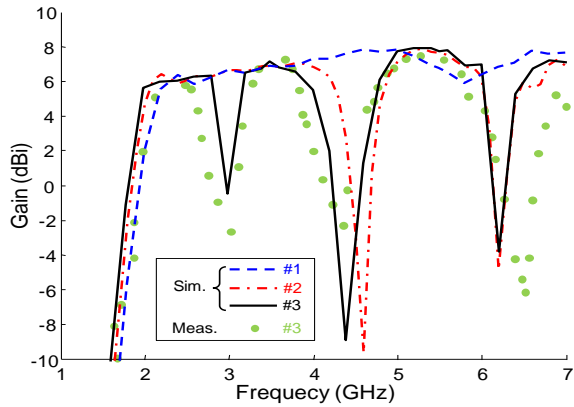conductive losses have been considered in the numerical modeling.

Fig. 8. The simulated and measured realized gain of the designs #1, #2, and #3, as depicted in Fig. 2.

In a systematic design process, it is very helpful for designers to relate geometrical parameters to critical design frequencies. In this context, we have developed an empirical formulae which relate the parameters of parasitic elements to the corresponding centre notch frequencies (namely, the lower frequency: f_L, the middle frequency: f_M, and the upper frequency: f_U). For this purpose, a series of simulations have been carried out by varying some parameters of the double-loop and split-ring elements as depicted in Fig. 9. It has been observed that the critical parameters mainly controlling the respective notch frequencies are L_1 (split-ring), g (gap between the loops), and L_4 (inner-loop). By employing a curve-fitting algorithm (available in MATLAB's Curve Fitting Toolbox), the following empirical equations in polynomial form have been derived based on a series of parametric studies using the CST simulator:

$$L_1 = 9.43 f_L^2 - 73.96 f_L + 167.4, \quad (1.a)$$

$$g = -929 f_M^3 - 1.72 \times 10^4 f_M^2 - 5.24 \times 10^4 f_M + 7.57 \times 10^4, \quad (1.b)$$

$$L_4 = -1.72 f_U - 20.35. \quad (1.c)$$

In Fig. 9, the critical parameters (L_1, g, L_4) are plotted against the particular notch frequencies (f_L, f_M, f_U), where a good agreement is observed

between the proposed formulae and the CST simulations. Hence, one can specify notch frequencies, and then obtain the associated antenna parameters by means of the design curves in Fig. 9. We remark that during parametric studies, only one parameter at a time has been varied while the others kept unchanged. Also, note that there has been negligible effect observed on the antenna's frequency response, except for each notch band while varying the corresponding dimension. That is, each parameter mainly affects the corresponding notch band as can be observed from Fig. 10.
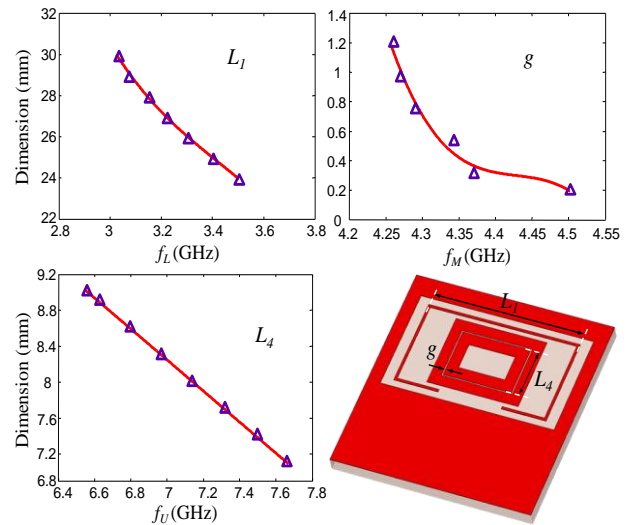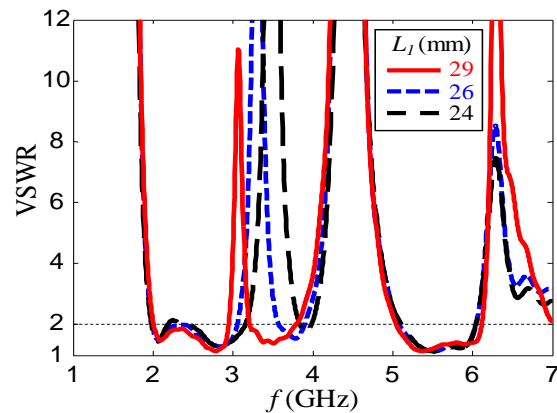

Fig. 9. The design curves for the critical parameters (L_1, g, L_4) vs. the centre notch frequencies: CST simulations (Δ) and the empirical formulae 1 (solid line).
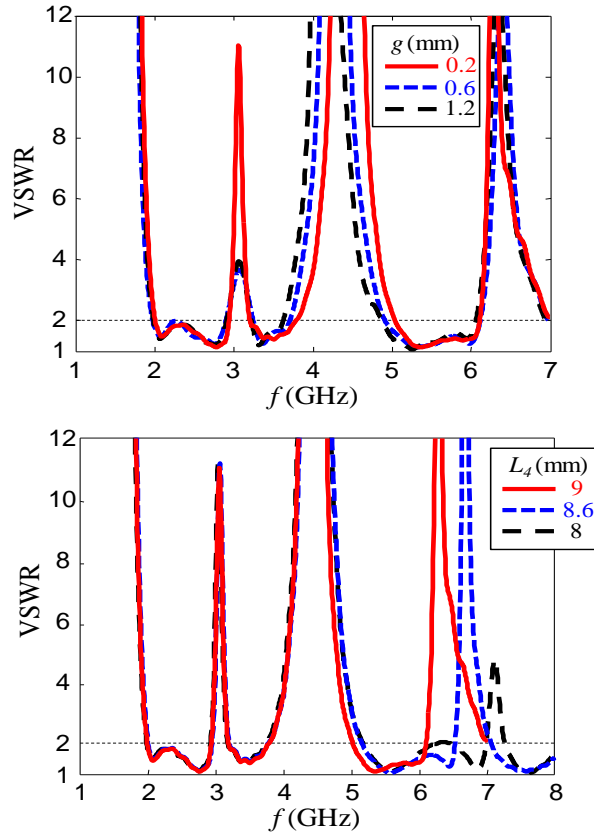
Fig. 10. The effects of the critical parameters (L_1, g, L_4) on the VSWR performance.

Furthermore, an Equivalent Circuit Model (ECM) for the triple-band antenna has been considered to serve as an additional design perspective. As depicted in Fig. 11, the proposed ECM is formed by integration of the circuit model for the loading elements (double-loop [14] and resonant split-ring) and the circuit model for the wide slot antenna alone [15]. Having constructed this simplistic model, the circuit parameters (R, L, C) have been extracted by means of a curve-fitting algorithm [19], based on the simulated VSWR characteristics of the triple-band antenna.

As can be seen from Fig. 12, the proposed ECM predicts the operational bands as well as the notch bands reasonably well. The discrepancies are probably due to the fact that this preliminary ECM does not include additional circuit elements representing coupling effects between the antenna elements. We note that those circuit element values will change if any physical parameter in the structure is altered. One can also develop

empirical formulae relating the ECM values with the corresponding physical design parameters [20].
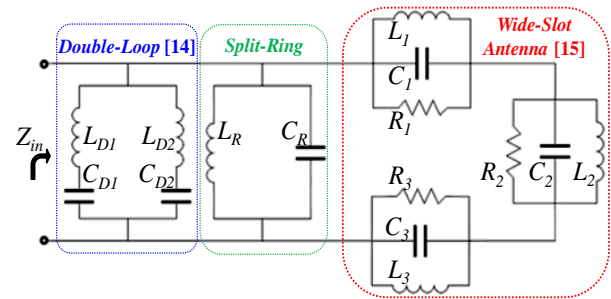

Fig. 11. The proposed equivalent circuit model for the triple-band antenna: C_1=11 pF, L_1=0.65 nH, R_1=50 Ω, C_2=4 pF, L_2=0.7 nH, R_2=25 Ω, C_3=0.7 pF, L_3=1.2 nH, R_3=45 Ω, L_R=0.07 pH, C_R=38 nF, L_{D1}=6.5 nH, C_{D1}=0.2 pF, L_{D2}=8.7 nH, C_{D2}=0.07 pF.
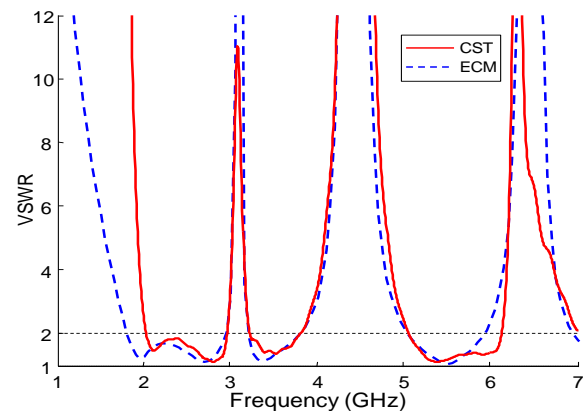

Fig. 12. The comparison of VSWR characteristics for the triple-band antenna: CST simulations vs. Equivalent Circuit Model (ECM).

IV. CONCLUSION

In the paper, a novel printed antenna has been proposed for interference-free triple-band WiMAX/WLAN operations. The printed antenna coupled to a microstrip feedline has a rectangular wide-slot element with the parasitic double-loop and split-ring elements. While the slot element alone shows wideband VSWR performance, the triple-band performance is achieved via utilizing parasitic elements within the wideband antenna design. Those parasitic loadings play a key role in generating the notch bands, which avoid possible interferences from dispensable bands and cover

only the assigned bands for WiMAX and WLAN operations. The proposed antenna is moderate-size, low-loss, low-cost, and more importantly offers flatter and better gain profile (6.5 dBi on the average) as compared to its counterparts to our best knowledge. The measurements of the fabricated antenna have been demonstrated to agree with the corresponding CST simulations quite well. Besides the antenna's satisfactory performance, the introduced empirical formulae as well as the proposed equivalent circuit model can be considered as additional contributions of this research to assist engineering design.

ACKNOWLEDGMENT

REFERENCES

[1] C. Y. Pan, T. S. Horng, W. S. Chen, and C. H. Huang, "Dual wideband printed monopole antenna for WLAN/WiMAX applications," *IEEE Antennas Wireless Propag. Lett.*, vol. 6, pp. 149-151, 2007.

[2] D. Zhou, R. A. Abd-Alhameed, A. G. Alhaddad, C. H. See, J. M. Noras, P. S. Excell, and S. Gao, "Multi-band weakly ground-coupled balanced antenna design for portable devices," *IET Science, Measurement & Technology*, vol. 6, no. 4, pp. 306-310, 2012.

[3] L. Hu and W. Hua, "Wide dual-band CPW-fed slot antenna," *Electron. Lett.*, vol. 47, no. 14, pp. 789-790, 2011.

[4] M. H. B. Ucar and Y. E. Erdemli, "Microstripline-coupled printed wide-slot antenna with loop loadings for dual-band WiMAX/WLAN operations," *IEEE Int. Symp. Antennas Propagat.*, Chicago, IL, pp. 1-2, July 2012.

[5] T. Wang, Y. Z. Yin, J. Yang, Y. L. Zhang, and J. J. Xie, "Compact triple-band antenna using defected ground structure for WLAN/WiMAX applications," *Prog. Electromagn. Res. Lett.*, vol. 35, pp. 155-164, 2012.

[6] X. Q. Zhang, Y. C. Jiao, and W. H. Wang, "Compact wide tri-band slot antenna for WLAN/WiMAX applications," *Electron. Lett.*, vol. 48, no. 2, pp. 64-65, 2012.

[7] H. W. Liu, C. H. Ku, and C. F. Yang, "Novel CPW-fed planar monopole antenna for WiMAX/WLAN applications," *IEEE Antennas Wireless Propag. Lett.*, vol. 9, pp. 240-243, 2010.

[8] Z. X. Yuan, Y. Z. Yin, Y. Li, B. Ding, and J. J. Xie, "Multiband printed and double-sided dipole antenna for WLAN/WiMAX applications,"

Microwave Opt. Technol. Letts., vol. 54, pp. 1019-1022, 2012.

[9] P. Wang, G. J. Wen, and Y. Huang, "Compact CPW-fed planar monopole antenna with triple-band operation for WLAN/WiMAX applications," *Applied Computational Electromagnetic Society (ACES) Journal*, vol. 27, no. 8, pp. 691-696, June 2012.

[10] P. Shu and Q. Feng, "Design of a compact quad-band hybrid antenna for compass/WiMAX/WLAN applications," *Prog. Electromagn. Res.*, vol. 138, 585-598, 2013.

[11] A. Dadgarpour, A. Abbosh, and F. Jolani, "Planar multiband antenna for compact mobile transceivers," *IEEE Antennas Wireless Propag. Lett.*, vol. 10, pp. 651-654, 2011.

[12] Y. Wang, J. Li, and L. X. Ran, "An equivalent circuit modeling method for ultra-wideband antennas," *Prog. Electromagn. Res.*, vol. 82, pp. 433-445, 2008.

[13] Y. S. Wang and S. J. Chung, "A short open-end slot antenna with equivalent circuit analysis," *IEEE Trans. Antennas and Propag.*, vol. 58, no. 5, pp. 1771-1775, 2010.

[14] X. F. Luo, P. T. Teo, A. Qing, and C. K. Lee, "Design of double-square-loop frequency-selective surfaces using differential evolution strategy coupled with equivalent-circuit model," *Microwave Opt. Technol. Letts.*, vol. 44, pp. 159-162, 2005.

[15] I. Pele, A. Chousseaud, and S. Toutain, "Simultaneous modeling of impedance and radiation pattern antenna for UWB pulse modulation," *IEEE Int. Symp. Antennas Propagat.*, Monterey, CA, vol. 2, pp. 1871-1874, June 2004.

[16] J. R. Kelly, P. S. Hall, and P. Gardner, "Band-notched UWB antenna incorporating a microstrip open-loop resonator," *IEEE Trans. Antennas and Propag.*, vol. 59, no. 8, pp. 3045-3048, 2011.

[17] J. Y Sze and K. L. Wong, "Bandwidth enhancement of a microstrip-line-fed printed wide-slot antenna," *IEEE Trans. Antennas and Propag.*, vol. 49, no. 7, pp. 1020-1024, 2001.

[18] C. A. Balanis, "Antenna theory analysis and design," 3rd ed., *New York: Wiley-Interscience*, pp. 1029, 2005.

[19] M. H. B. Ucar, A. Sondas, and Y. E. Erdemli, "Dual-band loop-loaded printed dipole antenna with a wideband microstrip balun structure," *Applied Computational Electromagnetic Society (ACES) Journal*, vol. 27, no. 6, pp. 458-465, June 2012.

[20] Y. E. Erdemli, K. Sertel, R. A. Gilbert, D. E. Wright, and J. L. Volakis, "Frequency selective surfaces to enhance performance of broadband reconfigurable arrays," *IEEE Trans. Antennas Propag.*, vol. 50, no. 12, pp. 1716-1724, 2002.

Mustafa H. B. Ucar received his B.S., M.S., and Ph.D. degrees from Kocaeli University, Kocaeli, Turkey, all in Electronics and Computer Education Department in 2004, 2007, and 2013, respectively. He currently serves as an Assistant Professor in the Department of Information Systems Engineering, Kocaeli University, Turkey. His research interests include numerical analysis and design of reconfigurable antennas/arrays/EM filters and frequency selective surfaces.

Yunus E. Erdemli received his B.S. degree in Electrical Engineering from Middle East Technical University, Ankara, Turkey, in 1992, and the M.S. and Ph.D. degrees from the University of Michigan, Ann Arbor, both in Electrical Engineering, in 1996 and 2002, respectively. During 1994-2002, he was a graduate Research Assistant at the University of Michigan Radiation Laboratory, Ann Arbor, where he also served as a Postdoctoral Research Associate. He currently serves as a Professor in the Department of Biomedical Engineering, Kocaeli University, Turkey. His research interests include biomedical applications, numerical analysis and design of conformal and reconfigurable antenna arrays, frequency selective surfaces/volumes and metamaterials for various communication applications.